Supporting Information

Supporting Information for: Quantification, Diel Variation and Photochemistry of Inorganic Chlorine Trace Gases in Continental Germany

Lasse Moormann,[a] John N. Crowley, *[b] Friederike Fachinger [a] and Frank Drewnick [a]

A Formation of chlorine-containing species from secondary ion chemistry

$ICl NO_3^-$

Due to the high correlation of r^2 = 0.86 between $ClONO_2$ and $ClNO_2$ throughout the campaign, we initially suspected that the reaction of $ClNO_2$ with IO_X^- ions in the IMR of the CIMS instrument was responsible for the observed $ICl NO_3^-$ signal. IO_X^- (x = 1 to 3) is formed from the reaction of the reagent ions I^- and IH_2O^- with O_3 inside the IMR and is known to be involved in (unwanted) secondary ion reactions when using iodide as primary ions [1-4]. In order to investigate whether the $ICl NO_3^-$ measurements were an artefact of secondary ion-chemistry, we conducted a series of laboratory experiments with elevated levels of O_3 to study the formation of $ICl NO_3^-$ via reactions R17a and R17b under humidified and dry conditions in the IMR. In these experiments, a constant amount of $ClNO_2$ (~1 ppbv) was added to the CIMS inlet with addition of O_3 between 0 and 170 ppbv, thereby varying the amount of IO_X^- in the IMR.

$$ICl NO_2^- + IO_X^- \rightarrow ICl NO_3^- + IO_{X-1}^-, x = 1-3 \quad \text{(R17a)}$$

$$ClNO_2 + IO_X^- \rightarrow ICl NO_3^- + O_{X-1}^-, x = 1-3 \quad \text{(R17b)}$$

We found that neither the $ClNO_2$ mixing ratio (measured as $ICl NO_2^-$) nor that of $ICl NO_3^-$ had changed significantly when O_3 was added with mixing ratios up to 170 ppbv under both dry and wet conditions. The IO_X^- signal increased linearly (Fig. S9a) over this range of O_3 mixing ratios, which exceeds those encountered during the BISTUM24 campaign (8 to 67 ppbv). We therefore conclude that the measurement of $ClONO_2$ is not a measurement artefact and that $ClONO_2$ was indeed present at the mixing ratios reported.

$IHClO_2^-$

In addition to $IHClO^-$ (the detected ion cluster of HOCl in the CIMS), $IHClO_2^-$ was detected at a signal intensity of 25% that of $IHClO^-$. A potential source of this ion is the reaction between atmospheric peroxyhypochlorous acid (HOOCl) and iodide in the IMR of the CIMS instrument. A recent study has highlighted the potential contribution of HOOCl to chlorine chemistry in the Antarctic vortex [5], where its source is the heterogeneous reaction between dichlorine dioxide (Cl_2O_2) and HCl [6]. While this may be possible in the cold polar vortex, where Cl_2O_2 is stable, this process will certainly be insignificant in the troposphere due to thermolability [7]. Theoretical studies [8] propose the existence of HOOCl under tropospheric conditions though it has never been detected experimentally there. Thus, we consider the formation of $IHClO_2^-$ as being due to secondary ion chemistry of HOCl or HCl with IO_X^- in the IMR as more likely than detection of atmospheric HOOCl.
We investigated the possible involvement of IO_X^- due to enhanced O_3 levels (i.e., IO_X^-) in the formation of $IHClO_2^-$ by mixing a flow of HOCl with O_3 (0 to 200 ppbv) under humid and dry IMR conditions and found that both $IHClO_2^-$ and $IHClO^-$ were detected. The $IHClO^-$ signal increased with added O_3, while the $IHClO_2^-$ signal remained constant (Fig. S9c). In a further experiment in the absence

[a] Multiphase Chemistry Department, Max Planck Institute for Chemistry, Mainz, 55128, Germany
[b] Atmospheric Chemistry Department, Max Planck Institute for Chemistry, Mainz, 55128, Germany

of HOCl, but with high amounts of HCl (not quantified, but significantly above the detection limit), both $IHClO^-$ and $IHClO_2^-$ signals increased with added O_3 (and thus with higher IO_X^- counts, Fig. S9d). This indicates the direct oxidation and cluster formation of HCl to $IHClO^-$ and $IHClO_2^-$ (R18), in contrast to a successive oxidation scheme like for $IHNO_3^-$ [3].

$$\mathrm{HCl} \xrightarrow{\mathrm{IO}_x^-} IHClO_2^- \; or \; \mathrm{IHOCl}^-, x = 1-3 \qquad \text{(R18)}$$

It appears very likely that atmospheric HCl and O_3 are the main source of $IHClO^-$ and $IHClO_2^-$ in the IMR. However, the relatively low O_3 levels from the ambient measurements in this work are not expected to influence the $IHClO^-$ signal significantly, hence, a correction was not applied.

Figures

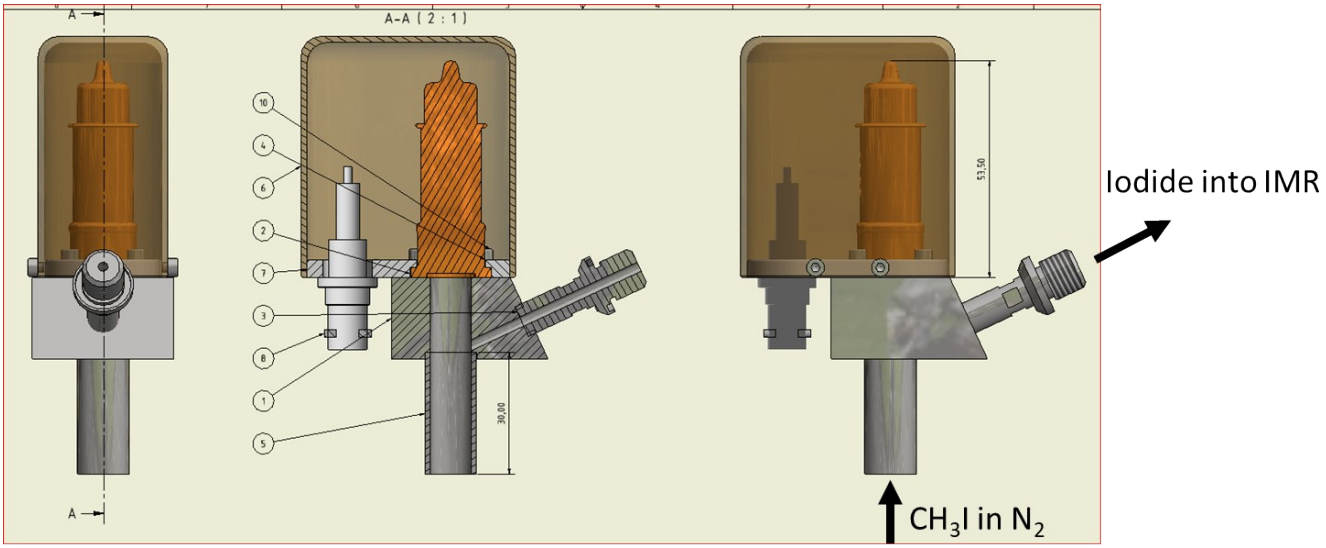

Figure S1: The VUV lamp (orange striped) is capsulated by a 3D-printed plastic (brownish box). The capsulating plastics has a hole to observe ignition of the lamp. The lamp radiates downwards into the grey tube contrary to the reagent gas flow.

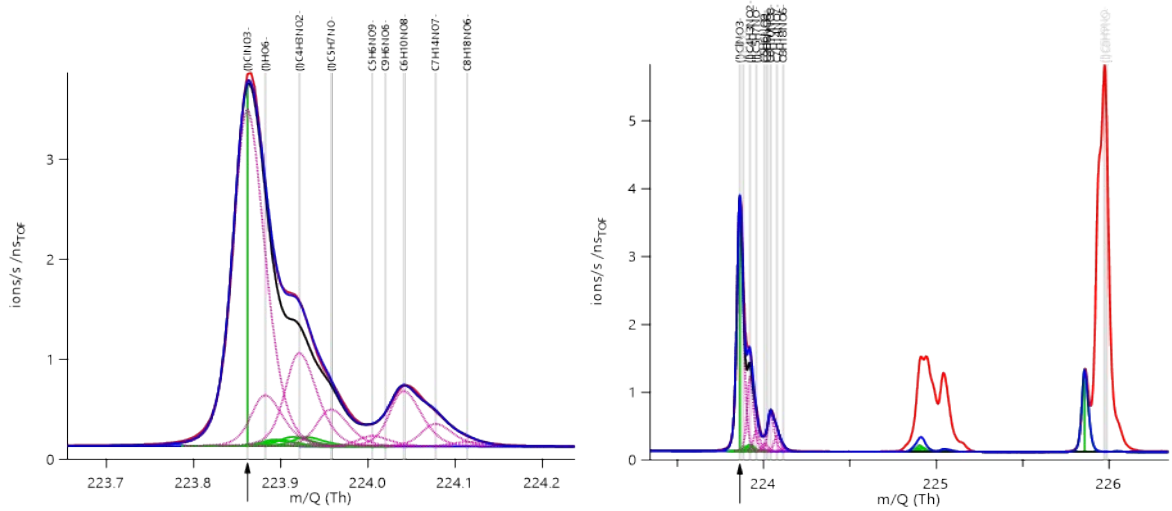

Figure S2: The HR mean mass spectra at m/z 224 of the "marine-anthropogenically" influenced air mass shows unambiguous detection of ClONO2 as IClNO3- in the HR-spectra (marked with green bar, left) as well as in the isotope ratio of exactly 3:1 from $I^{35}ClNO_3^-$ (at m/z 224)-to- $I^{37}ClNO_3^-$ (at m/z 226, right). The raw (red) and fitted (blue) mass spectra are plotted with individual assigned ions at the respective m/z (violet) and isotopes from lower m/z (green).

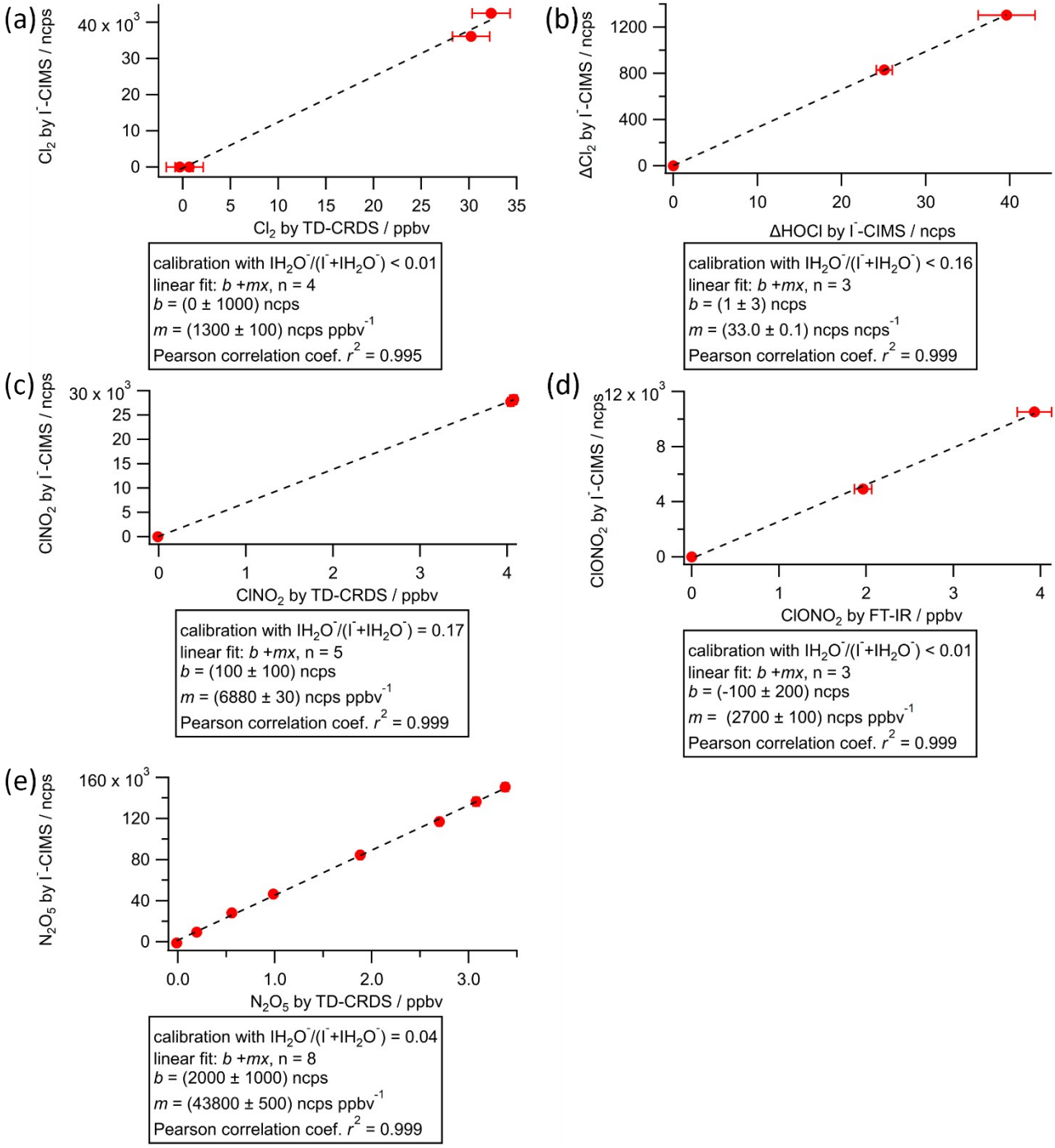

Figure S3: Calibration curves (red) for Cl_2 (a), HOCl (b), $ClNO_2$ (c), $ClONO_2$ (d) and N_2O_5 (e) with linear regressions (black dashed lines). Error bars represent the standard deviation of noise of data points in the calibration intervals. The uncertainties are for intercept *b* and slope *m* are given for one standard deviation of the fit. The overall measurement uncertainty is dominated by the uncertainty of the CRDS and FT-IR instrument (on the x-axis).

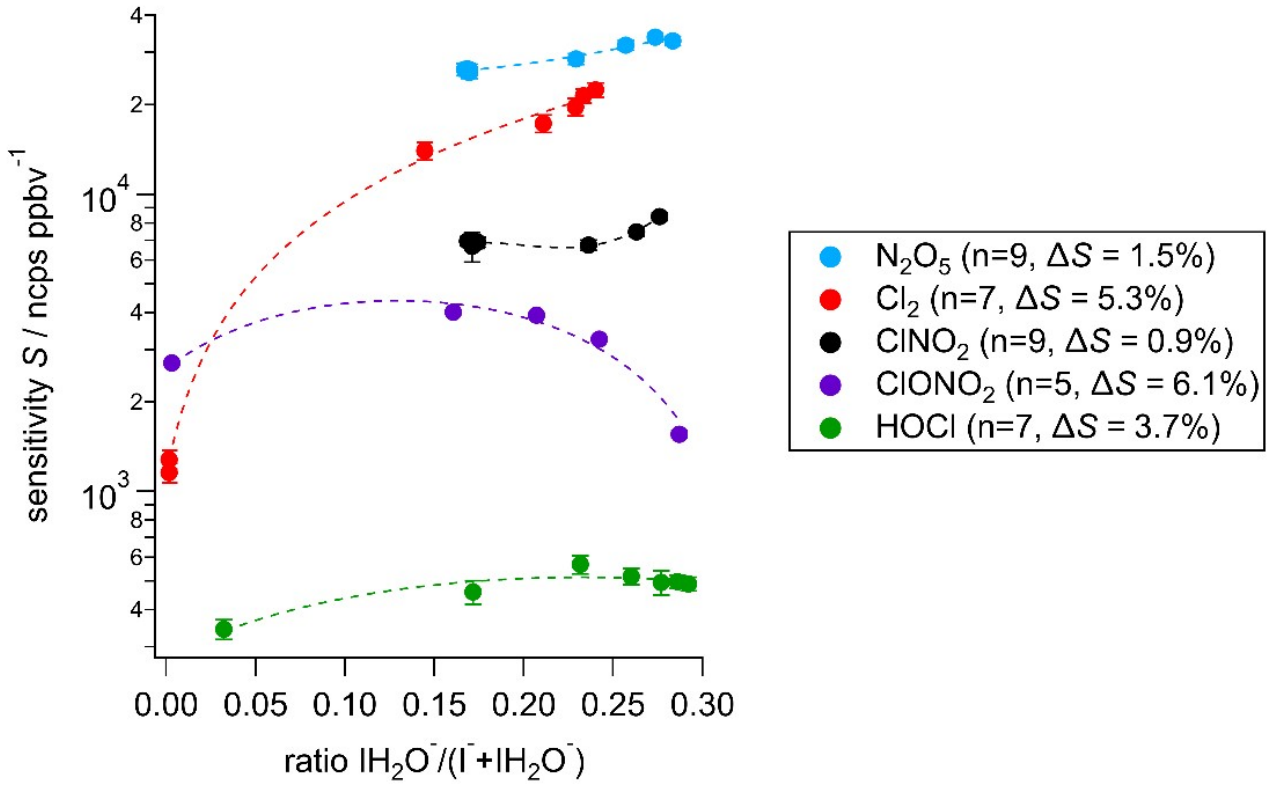

Figure S4: Sensitivity dependency on the $IH_2O^-/(I^- + IH_2O^-)$ ratio in the IMR for $ICINO_2^-$ (black), $IN_2O_5^-$ (light blue), ICl_2^- (red), $ICIONO_2^-$ (dark blue) and $IHOCl^-$ (green) derived from polynomial fits are valid for the covered humidity range, which sufficiently captures the humidity range of the field data.

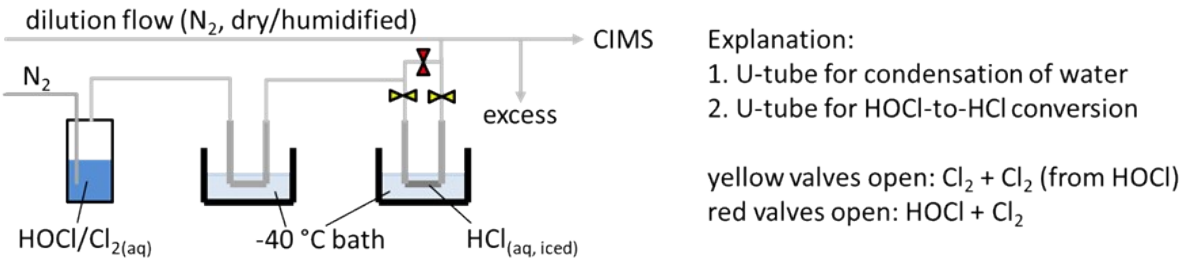

Figure S5: Experimental setup for the HOCl calibration with the CIMS. HOCl was converted to Cl_2 on an HCl/ice surface.

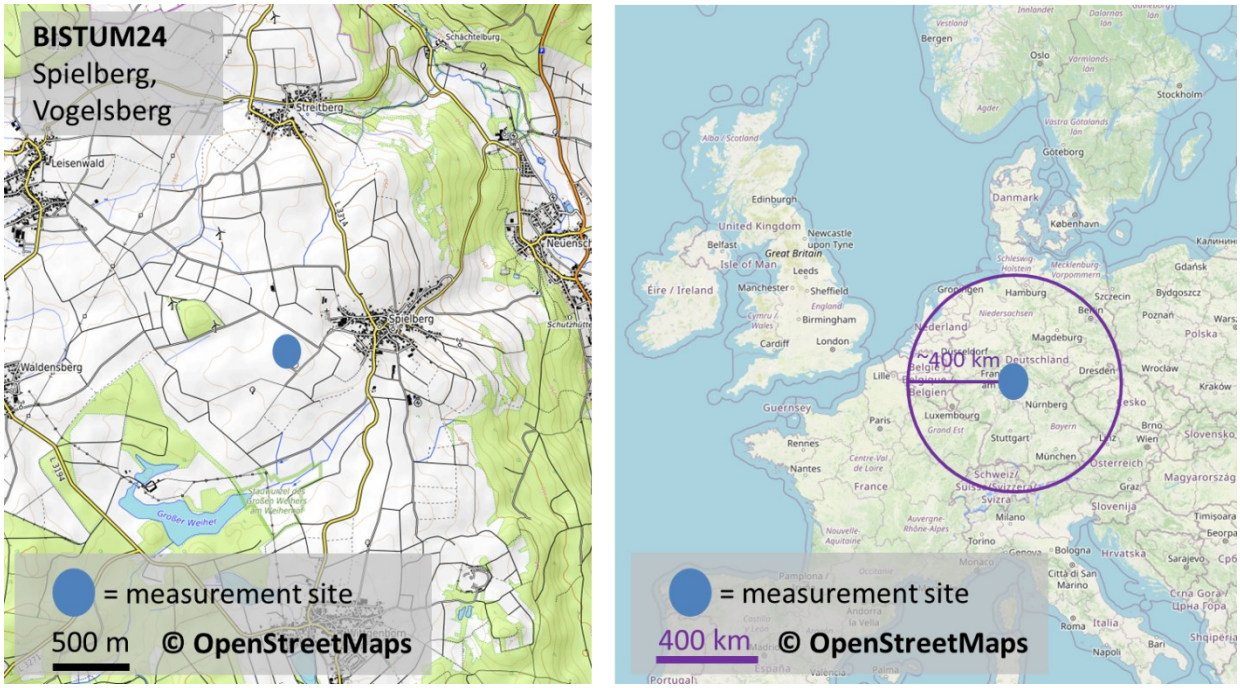

Figure S6: The field measurements took place in rural Spielberg, Hessen, Germany from June 6 to 22, 2024. Maps were publicly available from ©OpenStreetMaps via its Creative Commons licence.

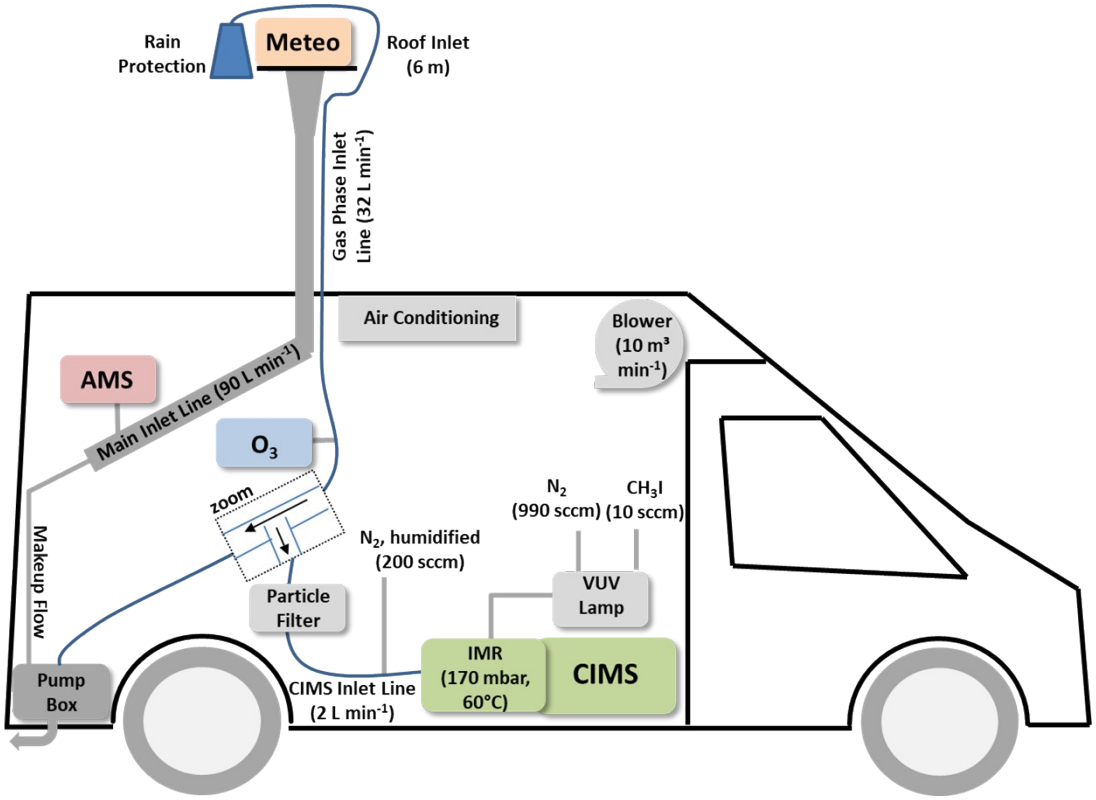

Figure S7: Schematic representation of MoLa with relevant instruments: AMS (red), O_3 monitor (blue), weather station for meteorological data (yellow) and CIMS (green) and separate tubing for aerosol and gas samples: stainless steel (grey), PTFE (blue). The figure was adapted from Drewnick et al.[9].

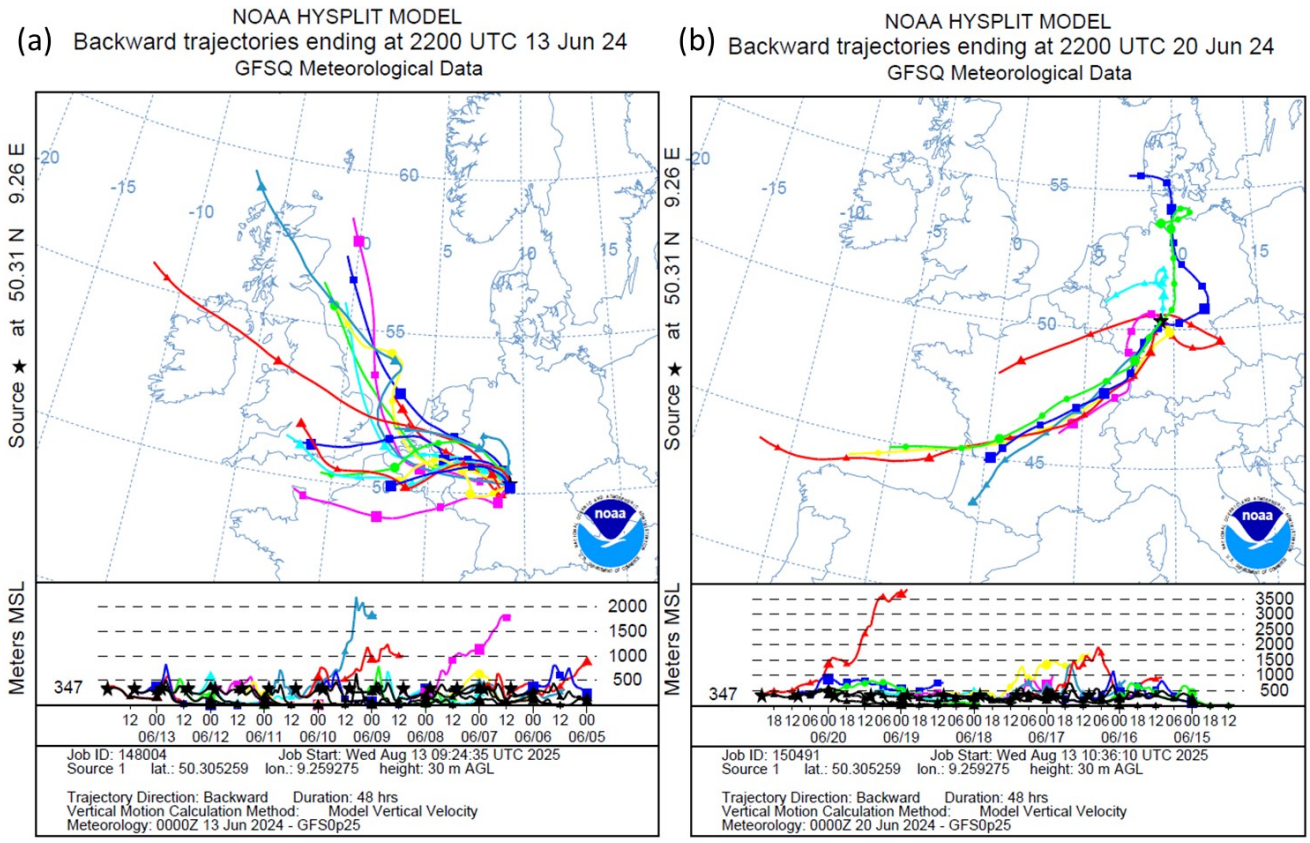

Figure S8: 48-h backward trajectories starting every 6 - 12 h from June 6 to 14, 2024 show a shallow advection rarely exceeding 500 m above mean sea level (MSL), while trajectories starting from June 16 to 21, 2024 originate from higher aspiration levels - usually from above 1000 m above mean sea level. The trajectories were calculated with the HySplit trajectory model [10, 11].

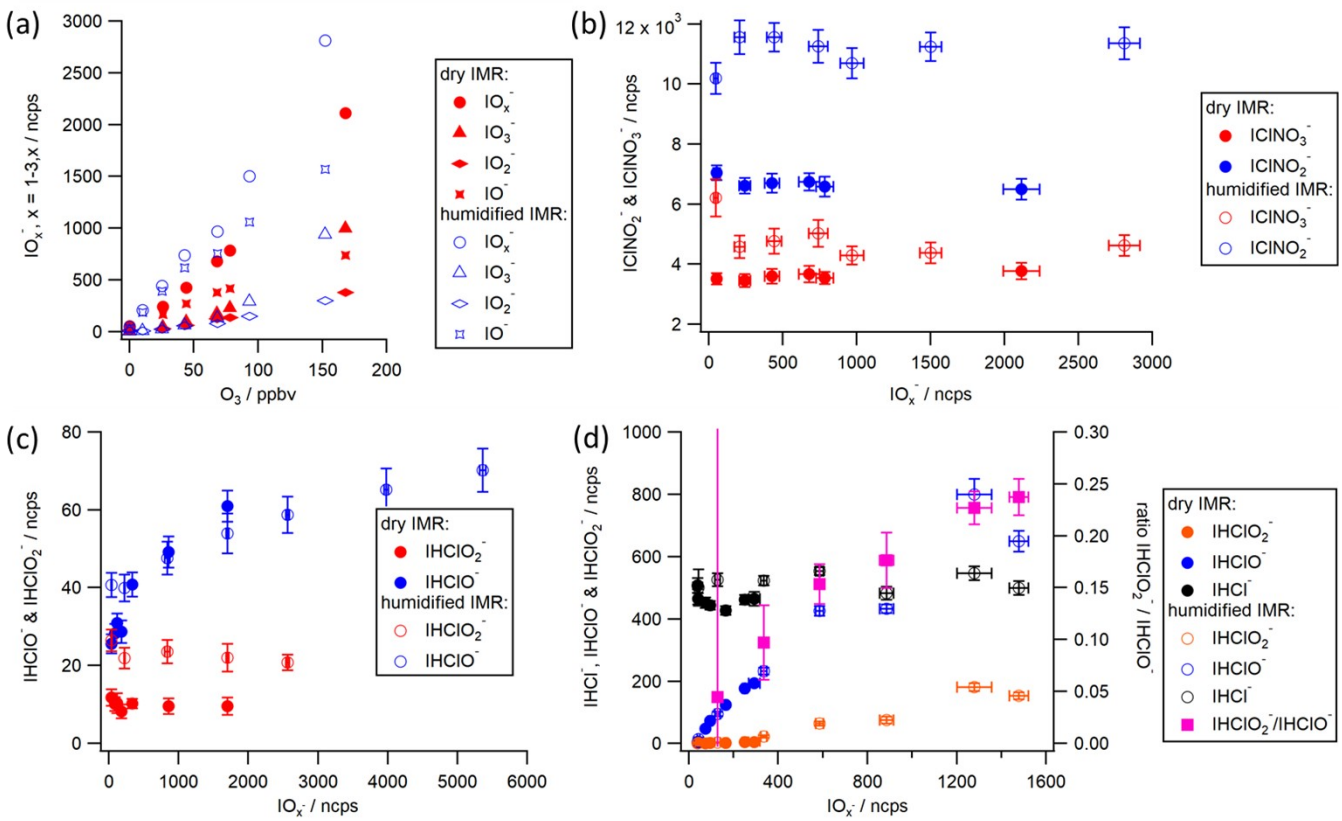

Figure S9: Overview of experiments to investigate secondary ion chemistry due to O_3 inside the IMR (ion molecule reactor) of the CIMS. The relationship between O_3 and IO_x^- is linear for a dry and humidified IMR, although the contribution to IO_x^- (x=1-3) changes with the amount of O_3 (a). (b) shows that no secondary ion chemistry formation of $ICINO_3^-$ is expected over a broad range of O_3 mixing ratios, neither for the humidified nor for the dry IMR case. In contrast, (c) indicates a significant increase of $IHClO^-$ with higher IO_x^- levels in the IMR, which is not the case for $IHClO_2^-$ as long as the HCl concentration in the IMR is below the detection limit. The same experiment with enhanced HCl levels is shown in (d), where the $IHClO_2^-$/$IHClO^-$ ratio increases with IO_x^- levels.

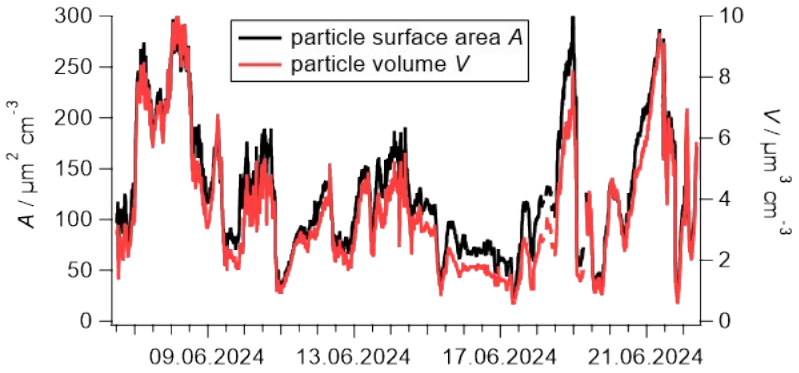

Figure S10: Time series of the particle surface area *A* and the particle volume *V* throughout the campaign. The nighttime mean (and standard deviation) A_{night} = (130 ± 65) µm^2 cm^{-3} agrees well with the campaign mean. Even with extreme *A* from 50 – 300 µm^2 cm^{-3}, photolysis of HOCl (~few hours) dominates heterogenous loss of HOCl on aerosol particles (with 2.2 – 15 days lifetime, respectively).

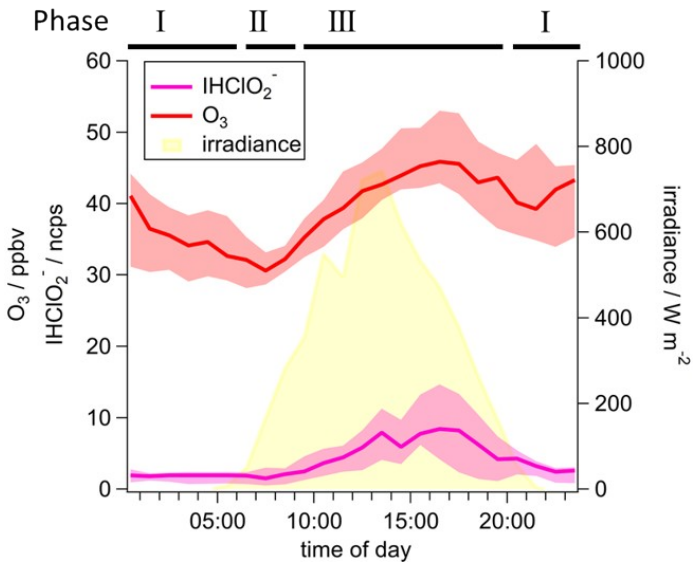

Figure S11: Diel cycle of IHO_2Cl- (pink) when O3 mixing ratios (red) are enhanced due to irradiance (yellow) Lines represent the median, the interquartile ranges are given as shaded area. The diel cycles only consider data from the "marine-anthropogenic" period of the BISTUM24 campaign.

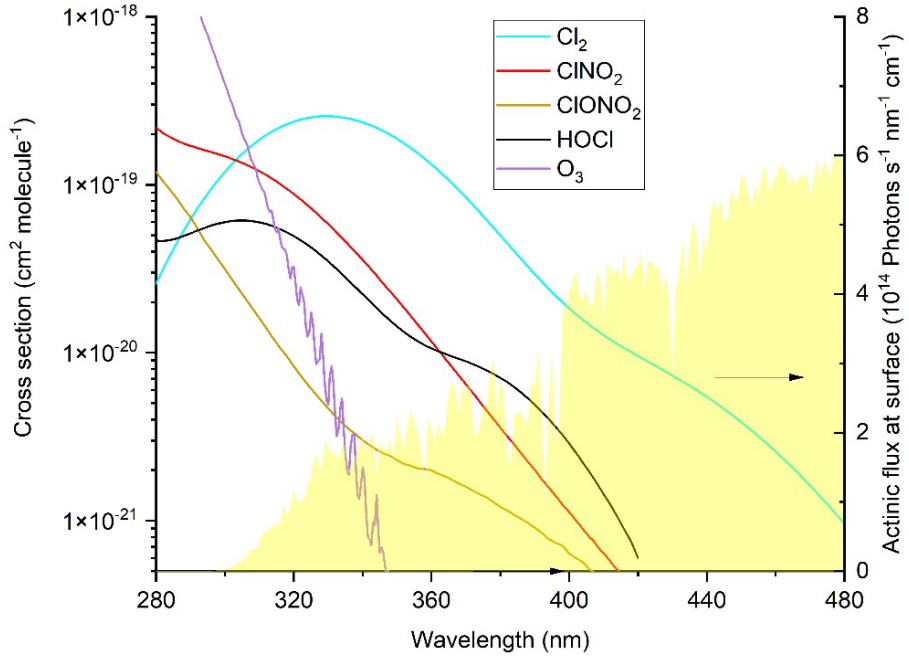

Figure S12: UV absorption spectra of the chlorine trace-gases detected in this study (Cl_2 (blue [12]), $ClNO_2$ (red [13]), $ClONO_2$ (bright green [14]) and HOCl (black [15]) and of O_3 (violet [16]). The actinic flux is shown for local noon (cloud free sky) on June 10th 2024 at the location of the BISTUM24 campaign [17].

References

1. R. Teiwes, J. Elm, M. Bilde and H. B. Pedersen, *Physical Chemistry Chemical Physics*, 2019, **21**, 17546-17554.
2. W. Zhang and H. Zhang, *Analytical Chemistry*, 2021, **93**, 8595-8602.
3. R. Dörich, P. Eger, J. Lelieveld and J. N. Crowley, *Atmospheric Measurement Techniques*, 2021, **14**, 5319-5332.
4. C. J. Young, S. Joudan, Y. Tao, J. J. B. Wentzell and J. Liggio, *Environmental Science & Technology Letters*, 2024, **11**, 1348-1354.
5. J.-U. Grooß, R. Müller, J. N. Crowley and M. I. Hegglin, *Communications Earth & Environment*, 2025, **6**.
6. D. O. De Haan and J. W. Birks, *The Journal of Physical Chemistry A*, 1997, **101**, 8026-8034.
7. M. Von Hobe, J. U. Grooß, R. Müller, S. Hrechanyy, U. Winkler and F. Stroh, *Atmospheric Chemistry and Physics*, 2005, **5**, 693-702.

8. T. J. Lee and A. P. Rendell, *The Journal of Physical Chemistry*, 1993, **97**, 6999-7002.
9. F. Drewnick, T. Böttger, S. L. von der Weiden-Reinmüller, S. R. Zorn, T. Klimach, J. Schneider and S. Borrmann, *Atmospheric Measurement Techniques*, 2012, **5**, 1443-1457.
10. A. F. Stein, R. R. Draxler, G. D. Rolph, B. J. B. Stunder, M. D. Cohen and F. Ngan, *Bulletin of the American Meteorological Society*, 2015, **96**, 2059-2077.
11. G. Rolph, A. Stein and B. Stunder, *Environmental Modelling & Software*, 2017, **95**, 210-228.
12. D. Maric, J. P. Burrows, R. Meller and G. K. Moortgat, *Journal of Photochemistry and Photobiology A: Chemistry*, 1993, **70**, 205-214.
13. B. Ghosh, D. K. Papanastasiou, R. K. Talukdar, J. M. Roberts and J. B. Burkholder, *The Journal of Physical Chemistry A*, 2012, **116**, 5796-5805.
14. J. B. Burkholder, R. K. Talukdar and A. R. Ravishankara, *Geophysical Research Letters*, 1994, **21**, 585-588.
15. IUPAC, *Journal*, 2025, DOI: http://iupac.pole-ether.fr.
16. L. T. Molina and M. J. Molina, *Journal of Geophysical Research: Atmospheres*, 1986, **91**, 14501-14508.
17. UCAR, TUV Calculator, https://www.acom.ucar.edu/Models/TUV/Interactive_TUV/, (accessed 15.06.2025, 2025).

